Energy transitions in superhydrophobicity: low adhesion, easy flow and bouncing

2008 J. Phys.: Condens. Matter 20 395005

(http://iopscience.iop.org/0953-8984/20/39/395005)

J. Phys.: Condens. Matter **20** (2008) 395005 (6pp) doi:10.1088/0953-8984/20/39/395005

Energy transitions in superhydrophobicity: low adhesion, easy flow and bouncing

Michael Nosonovsky[1] **and Bharat Bhushan**[2,3]

[1] Stevens Institute of Technology, Castle Point on Hudson, Hoboken, NJ 07030, USA
[2] Nanoprobe Laboratory for Bio- and Nanotechnology and Biomimetics (NLB^2), The Ohio State University, 201 West 19th Avenue, Columbus, OH 43210-1142, USA

E-mail: bhushan.2@osu.edu

Received 17 July 2008
Published 4 September 2008
Online at stacks.iop.org/JPhysCM/20/395005

Abstract
The concept of superhydrophobicity was introduced in the 1990s as a result of the investigation of the microstructure of extremely water-repellent plant leaves. Since that time, artificial superhydrophobic surfaces have been developed and implemented, stimulated by advances in nanotechnology, and giving one of the most successful examples of a bio-inspired technology transferred into engineering applications. Superhydrophobicity is usually defined as the ability of a surface to have (i) a very high water contact angle (CA) and (ii) low CA hysteresis. Here we argue that the ability of a water droplet to bounce off a surface constitutes a third property that is crucial for applications. Furthermore, this property is naturally related to the first two properties, since the energy barriers separating the 'sticky' and 'non-sticky' states needed for bouncing droplets have the same origin as those needed for high CA and for low CA hysteresis.

(Some figures in this article are in colour only in the electronic version)

1. Introduction

Biomimetic surfaces and materials attract the attention of scientists and engineers due to their unusual properties. Mechanical properties of many biological materials exceed those of engineered materials, while their production by living organisms and plants does not require high temperatures and pressures (Fratzl 2007). This is achieved by a design methodology that is radically different from conventional engineering design. Biological materials and surfaces are created by an iterative process leading to hierarchical organization, rather than on the basis of end-process specifications. This allows biological materials to adjust to changing conditions, and gives a potential for self-repair and cross-scale interactions that can deal with processes at different scale lengths. Scientists and engineers try to mimic natural materials and surfaces utilizing the so-called biomimetic approach.

One of the most successful examples of biomimetic surfaces involves the lotus effect, including roughness-induced superhydrophobicity and self-cleaning. Leaves of the lotus (*Nelumbo nucifera*) plant are known to be extremely water repellent due to their wax coating and surface roughness. In nature, water-repellency is found, besides in plants, in insects and bird feathers. It has a certain biological function, providing fitness to the environment of plants and organism and protecting them from contamination and pathogens, such as spores and conidia of pathogenic microorganisms, and infections (Barthlott and Neinhuis 1997, Wagner *et al* 2003). Recent advances in surface micro/nanopatterning have led to numerous attempts to create roughness-induced superhydrophobic surfaces for technical applications that require low adhesion, in particular, micro/nanodevices (Nosonovsky and Bhushan 2008a). Several lotus effect products have become commercially available on the market (Bhushan *et al* 2008). Both experimental studies of superhydrophobicity and theoretical issues such as adequate surface roughness characterization became a topic of active investigation (Nosonovsky and Bhushan 2008b, 2008d). New areas of applications have been suggested, such as energy conversion and conservation (Nosonovsky and

[3] Author to whom any correspondence should be addressed.

Bhushan 2008c), microfluidics (Blossey 2003), and underwater superhydrophobicity (Marmur 2006).

Superhydrophobicity is usually defined as the ability to have the static contact angle (CA) with water greater than 150°. In addition, it is recognized that a superhydrophobic surface should have low CA hysteresis, or the difference between the advancing CA (when water is added or the water front advances) and receding CA (when water is removed or the water front recedes). The CA is a measure of adhesion between water and the solid surface, so the greater the contact angle, the lower the adhesion. The CA hysteresis, on the other hand, is a measure of energy dissipation during the wetting/dewetting cycle, or during the flow of a droplet along the solid surface. Interactions in the bulk volume of a droplet, at the solid–liquid contact surface, and at the triple line (solid–liquid–vapor contact line) affect the dissipation. While the volume interactions due to viscosity can be eliminated in the quasi-static limit of a very slow motion, the surface and line interactions remain even in the case of a low velocity motion.

There is another wetting characteristic, in addition to a high CA and low CA hysteresis, which is of practical importance for water-repellency. This is the behavior of a droplet impacting a surface with a certain velocity. In some cases it can be bounced off a superhydrophobic surface in an almost elastic manner (Quéré 2005, Bartolo *et al* 2006). The kinetic energy of the droplet is stored in the surface deformation during the impact. A deformed droplet has a higher surface area and thus higher surface free energy. Therefore, during the impact when the droplet is deformed, it can accommodate the kinetic energy. It was suggested that the effect might be of practical interest for agriculture, in particular, for treating leaves with pesticides (Quéré 2005). Since the leaf is likely to repel the droplet, it will not be treated; in addition, the scattering of the droplets contaminates the soil. If small amounts of a polymer soluble in water (such as polyoxyethylene) are added to water (Bergeron *et al* 2000), the bulk viscosity of water remains the same; however, the so-called elongation viscosity (resistance of the liquid to large extensions) is high. Droplets of such a mixture do not bounce, and it has been used as an agricultural spray (Quéré 2005). On the other hand, the bouncing droplets are useful for waterproof fabrics or concrete that should preserve their dryness under rain.

The ability of a surface to bounce off droplets constitutes the third property of a superhydrophobic surface, in addition to high CA and low CA hysteresis, that is important for both biological and technical applications. However, this third property has received relatively little attention. In this paper, we quantify the bouncing ability of a surface and relate it to the surface roughness using theoretical and experimental considerations.

2. Theoretical background

2.1. Wenzel and Cassie states

When a liquid front propagates along a solid surface for a small distance δx (figure 1(a)) with the CA of θ_0, the change of surface free energy is given by $\delta E = \delta x \cos\theta_0 \gamma_{LV} + \delta x(\gamma_{SL} - \gamma_{SV})$, where γ_{SL}, γ_{SV}, and γ_{LV} are the solid–liquid, solid–vapor, and liquid–vapor interface energies (Israelachvili 1992). Setting $\delta E = 0$ yields the Young equation

$$\gamma_{LV} \cos\theta_0 = W \tag{1}$$

where $W = \gamma_{SL} - \gamma_{SV}$ is the work of adhesion. For a heterogeneous rough surface composed of patches with different surface roughnesses R_n and energies w_n, the change of energy is given by

$$\delta E = \delta x \gamma_{LV} \cos\theta + \delta x W_{ave} \tag{2}$$

$$W_{ave} = \sum_n f_n R_n w_n$$

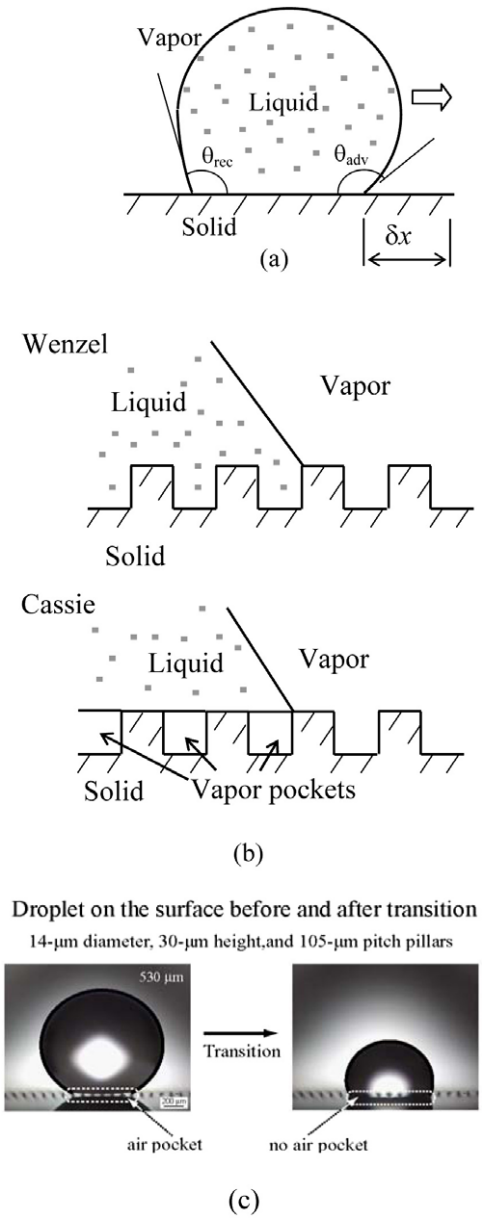

Figure 1. Geometry of the liquid advancement: (a) a droplet upon a solid surface exhibiting the advancing and receding CA, (b) schematic diagrams of Cassie and Wenzel states, and (c) the Cassie–Wenzel transition during evaporation of a droplet on a micropatterned surface (Jung and Bhushan 2008a).

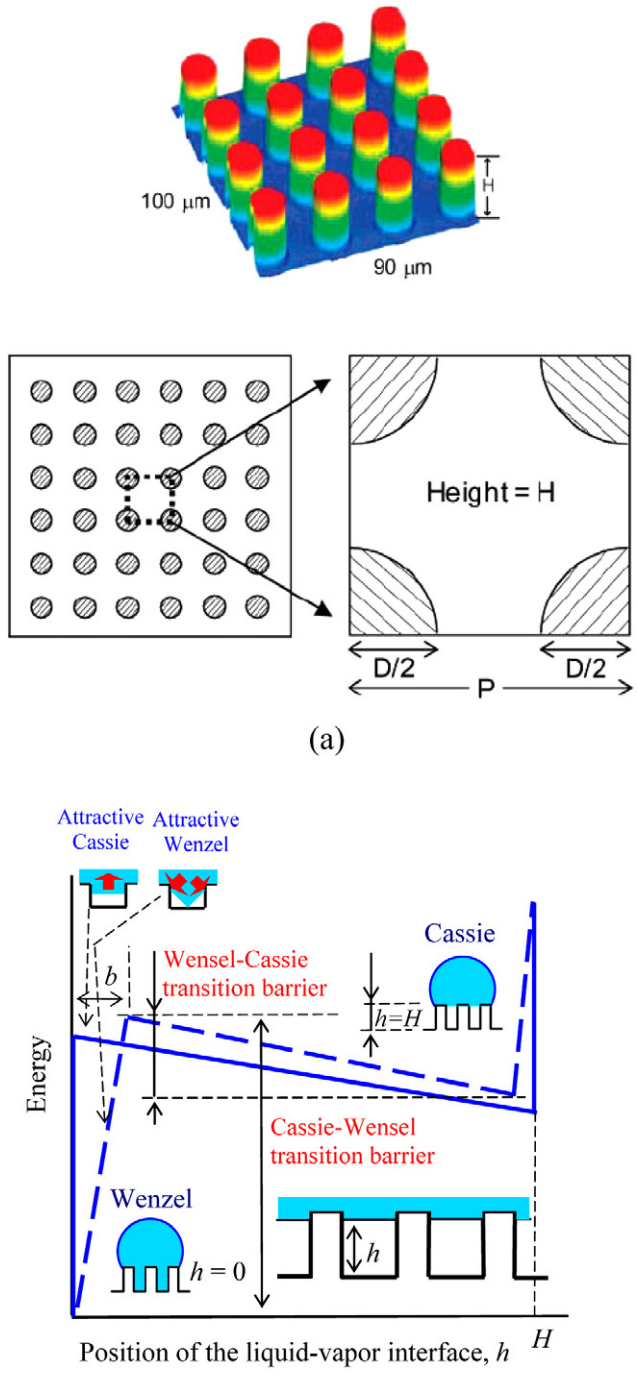

Figure 2. (a) Cylindrical flat-top columns on a micropatterned surface, and (b) energy barriers for the Cassie and Wenzel states. The energy is shown as a function of the height of the interface, h. The barrier is proportional to the column height H. The ideal case (solid line) involves an abrupt change of energy as the bottom of the surface is reached; however, a more realistic case (dashed line) has the offset b due to imperfections of the solid and liquid surfaces (e.g. surface waves).

where $W_{\rm ave}$ is the averaged value, f_n is the fraction of the patch ($\sum f_n = 1$), and R_n is the Wenzel roughness factor, equal to the ratio of the surface area to its flat projection ($R_n \geqslant 1$). The CA is then obtained by setting $\delta E = 0$ as

$$\cos\theta = \sum_n f_n R_n w_n. \tag{3}$$

In many practical situations, the surface consists of two fractions, one rough (with the roughness factor $R_{\rm f}$) and one smooth, so that equation (3) is reduced to

$$\cos\theta = R_{\rm f} f_0 \cos\theta_0 + f_1 \cos\theta_1 \tag{4}$$

where f_0 and f_1 are corresponding fractional areas (so that $f_0 + f_1 = 1$) and θ_1, θ_2, are contact angles of the two fractions. CA with a homogeneous rough surface ($f_0 = 1$, $f_1 = 0$) is given by the Wenzel equation that describes the homogeneous solid–liquid interface,

$$\cos\theta = R_{\rm f} \cos\theta_0. \tag{5}$$

The CA on a surface with air pockets trapped between the solid and liquid (the composite interface) is given by the Cassie–Baxter equation ($f_0 = f_{\rm SL}$, $\theta_1 = 180°$)

$$\cos\theta = R_{\rm f} f_{\rm SL} \cos\theta_0 - 1 + f_{\rm SL}. \tag{6}$$

The Wenzel and Cassie (or Cassie–Baxter) wetting regimes are sometimes treated as two-phase states with a certain energy barrier associated with the phase transition. Figure 1(b) shows schematic diagrams of a water front propagating along a micropatterned surface in the Wenzel and Cassie regimes. Figure 1(c) shows the transition of an evaporating droplet on a micropatterned surface as the droplet's radius decreases below a critical value. To maintain both a high CA and low CA hysteresis, the Cassie state is generally needed. The nature of the barriers between the two states remains a matter of discussion. The energy of the Cassie state can be lower or higher than that of the Wenzel state. The transition from Cassie to Wenzel states can often be initiated by applying pressure, mechanical vibration etc. The opposite transition is not normally observed (unless the surface energy is modified by a chemical reaction, irradiation or applying an electric potential) (Lafuma and Quéré 2003).

A schematic diagram showing a micropatterned superhydrophobic surface built of pillars of height H, diameter D and pitch P is presented in figure 2(a) (Bhushan *et al* 2007). The CA in the Wenzel and Cassie states is then given by

$$\begin{aligned} \cos\theta_{\rm W} &= \left(1 + \frac{\pi H D}{P^2}\right)\cos\theta_0 \\ \cos\theta_{\rm C} &= \frac{\pi D^2}{4P^2}(1 + \cos\theta_0) - 1. \end{aligned} \tag{7}$$

The energy barrier corresponding to the Cassie–Wenzel transition is given by the product of the height of the pillars, H, pillar perimeter, πD, pillar density, $1/P^2$, and area under the droplet, A_0, required to initiate the transition, and the corresponding change of the surface energy

$$\begin{aligned} \Delta E &= A_0 \frac{\pi H D}{P^2}(\gamma_{\rm SL} - \gamma_{\rm SV}) \\ &= -A_0 \frac{\pi H D}{P^2}\gamma_{\rm LV}\cos\theta_0 \end{aligned} \tag{8}$$

where A_0 is $\pi(R\sin\theta)^2$.

For a short pitch the net energy of the Cassie state is lower than that of the Wenzel state, whereas for larger values of the pitch the energy of the Wenzel state is lower (figure 2(b)). However, due to the energy barriers, a metastable Cassie state with a higher energy than the Wenzel state may be found.

2.2. *Impact of a droplet on a superhydrophobic surface*

The energy barrier of the Cassie–Wenzel transition can be estimated as the kinetic energy of the droplet. The kinetic energy of a droplet of radius R, mass m, and density ρ with velocity V is given by

$$E_{\text{kin}} = \frac{(4/3)\pi\rho R^3 V^2}{2} \tag{9}$$

while the free surface energy is given by

$$E_{\text{surf}} = 4\pi R^2 \gamma_{\text{LV}}. \tag{10}$$

In order for the surface deformation to accommodate the kinetic energy, the latter should be of the same order of magnitude as the former. For a water droplet ($\gamma_{\text{LV}} = 0.072$ N m^{-1}, $\rho = 1000$ kg m^{-2}) of $R = 1$ mm, the corresponding impact velocity is $V = 0.66$ m s^{-1}. The ratio of the kinetic and surface energies (or inertial to the capillary forces) is also characterized by the nondimensional Weber number

$$We = \frac{\rho R V^2}{\gamma_{\text{LV}}}. \tag{11}$$

Small *We* corresponds to low kinetic energy in comparison with the free surface energy. If the impact velocity is high (high *We*), implying that impact time is short, a thin film of compressed air could form at the surface, which facilitates bouncing. On the other hand, if the impact velocity (and *We*) is too high, the surface tension cannot accommodate the kinetic energy, or the Cassie–Wenzel transition can occur and the droplet sticks to the surface.

3. Analysis of experimental data

Jung and Bhushan (2008a, 2008b) studied two series of patterned Si surfaces, covered with a monolayer of hydrophobic tetrahydroperfluorodecyltrichlorosilane (CA with a nominally flat surface, $\theta_0 = 109°$, advancing and receding CA $\theta_{\text{adv0}} = 116°$ and $\theta_{\text{rec0}} = 82°$), formed by flat-top cylindrical pillars. Series 1 had pillars with the diameter $D = 5$ μm, height $H = 10$ μm and pitch values $P = (7, 7.5, 10, 12.5, 25, 37.5, 45, 60,$ and $75)$ μm, while series 2 had $D = 14$ μm, $H = 30$ μm and $P = (21, 23, 26, 35, 70, 105, 126, 168,$ and $210)$ μm. The series were designed in this manner to isolate the effect of the pitch, pitch-to-height and pitch-to-diameter ratios. The contact angle and contact angle hysteresis of millimeter-sized water droplets upon the samples were measured. In addition, the contact angle and the Wenzel–Cassie transition during evaporation of microdroplets were studied (figure 3(a)).

It was found that for small P the droplets were in the Cassie state sitting on top of the pillars, whereas with increasing P the transition to the Wenzel state occurred. The transition occurs at values of the pitch much greater than the intersection of the energy lines for the two states. Therefore, the droplet was in a metastable Cassie state, separated by an energy barrier from the Wenzel state (corresponding to lower energy).

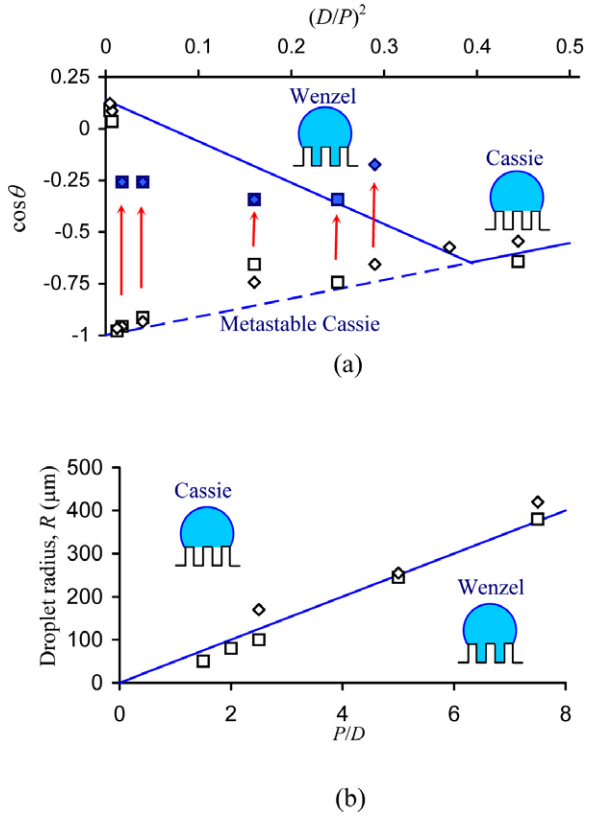

Figure 3. (a) Receding CA for macrodroplets (squares for the first and diamonds for the second series) and for evaporating microdroplets (blue/filled) and the theoretical values for the Cassie and Wenzel states. (b) The droplet radius R at which the transition occurs is linearly proportional to P/D. This is because the area A_0 in equation (8) is proportional to R^2. The fit (solid line) is shown for $RD/P = 50$ μm.

For evaporating droplets, the Cassie–Wenzel transition occurred when the droplet radius decreased below a certain critical value. The droplet radius, R, at the Cassie–Wenzel transition was found to be proportional to P/D (or P/H, since the height of the columns was proportional to their diameter) (figure 3(b)). On the other hand, the transition occurs as the vibrational energy of the droplet, E_{vib}, exceeds the energy barrier associated with the transition. The vibrational energy of the droplet (Johnson and Dettre 1964, Li and Amirfazli 2006, Bormashenko *et al* 2008) is the energy associated with the vibration of the droplet due to surface waves, thermal vibration, etc. Assuming $E_{\text{vib}} = \text{const}$, the proportionality of P/D and R suggests that the barrier ΔE given by equation (8) is proportional to the RD/P or (RH/P). This is indeed true, since the area under the droplet $A_0 = \pi(R\sin\theta)^2$. Substituting $\sin^2\theta = 0.1$, $\cos\theta_0 = \cos 109° = -0.33$, $\gamma_{\text{LV}} = 0.072$ J m^{-2} in equation (8) and taking the observed value $RD/P = 50$ μm yields an estimated value of the vibrational energy $E_{\text{vib}} = \Delta E = 1.2 \times 10^{-10}$ J.

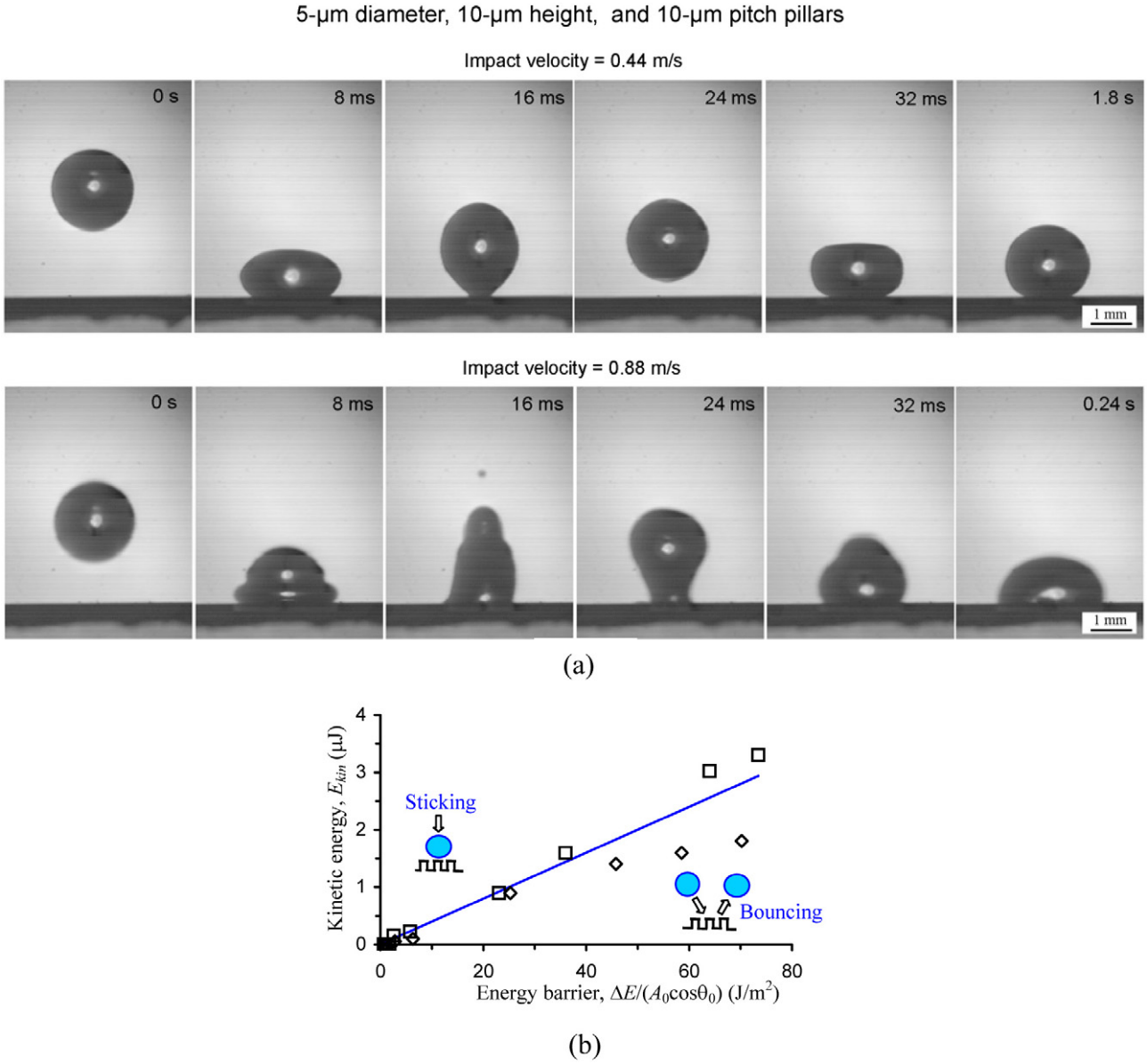

Figure 4. Bouncing droplets: (a) snapshots of a droplet with $R = 1$ mm hitting a micropatterned surface at two different velocities, showing sticking and bouncing (Jung and Bhushan 2008b), and (b) dependence of the kinetic energy of a droplet that provides the regime transition upon the energy barrier calculated from equation (8). The fit (solid line) is shown for $A_0 = 0.12$ mm^2.

Jung and Bhushan (2008b) also investigated the impact of water droplets with 5 μl volume (about 1 mm radius) upon the same series of surfaces. It was found that droplets impacting the surface with low velocity bounced off the surface, whereas those having high impact velocity stuck to the surface (figure 4(a)). Sticking was associated with being in the Wenzel state with a large solid–liquid contact area, while the droplets that bounced off the surface were in the Cassie state with an air pocket under them. Thus the energy barrier of the Cassie–Wenzel transition can be estimated as the kinetic energy of the droplets. Figure 4(b) shows the dependence of the kinetic energy corresponding to the transition, E_{kin}, on $\Delta E/(A_0 \cos\theta_0)$ calculated from equation (8). It is observed that the dependence is close to linear, however, the series of smaller pillars has larger energies of transition. The value of A_0 is in the range 0.11 mm^2 $< A_0 <$ 0.18 mm^2 for series 1 and 0.05 mm^2 $< A_0 <$ 0.11 mm^2 for series 2, which is of the same order as the actual area under the droplet.

These results suggest that the energy barrier for the Cassie–Wenzel transition is given by equation (8) and is proportional to the area under the droplet. For droplets sitting on the surface or evaporating, the transition takes place when the size of the barrier decreases to the value of the vibrational energy, approximately $E_{\text{vib}} = 10^{-10}$ J, which was estimated from the energy barrier. This may happen because the size of the droplet is decreased or because the pitch between the pillars that cover the surface is increased. A different way to overcome the barrier is to hit the surface with a droplet with a certain kinetic energy.

The vibrational energy E_{vib} also plays a role in overcoming energy barriers that lead to CA hysteresis during liquid flow (Johnson and Dettre 1964). To estimate the effect

of the energy barriers on CA hysteresis we assume, based on equation (1), that the difference between the advancing and receding CA is given by

$$\cos\theta_{\mathrm{rec}} - \cos\theta_{\mathrm{adv}} = \Delta W/\gamma_{\mathrm{LV}} \tag{12}$$

where ΔW corresponds to the energy barrier associated with the wetting–dewetting cycle. Assuming that this energy barrier is of the same order as the vibrational energy per contact area, $\Delta W = E_{\mathrm{vib}}/A_0$, and taking $A_0 = 0.1$ mm^2, we end up with $\Delta W = 10^{-3}$ J m^{-2}. For water ($\gamma_{\mathrm{LV}} = 0.072$ J m^{-2}), equation (12) leads to a realistic value of CA hysteresis on a superhydrophobic surface $\cos\theta_{\mathrm{rec}} - \cos\theta_{\mathrm{adv}} = 0.014$. This number provides an estimate for CA hysteresis in the limit of small energy barriers comparable with E_{vib}. The values that provide energy barriers due to so-called adhesion hysteresis and the density of the solid–liquid–vapor contact line that provides additional pinning are dependent upon the solid–liquid contact area. These values for a micropatterned surface were found to be between 0.0144 and 0.440 (Bhushan *et al* 2007), thus showing a good agreement with the value calculated based on E_{vib} as the lower limit. This indicates that the value of U is relevant for both the Cassie–Wenzel regime transition and CA hysteresis.

4. Conclusions

A superhydrophobic surface is characterized by three properties. First, it should have a high CA and thus low adhesion with a water droplet. Second, a water droplet should flow easily along the surface with small energy dissipation, and thus CA hysteresis should be low. The third property, which has received less attention, although it is important for many applications, is the ability to repel impacting droplets. This third property should be taken into consideration in the design of water-repellent surfaces. We have shown that these properties are related to energy barriers associated with the transition between the Cassie and Wenzel wetting states. Experimental data for droplets on patterned surfaces, evaporating microdroplets and droplets impacting the surface show that the nature of the energy barriers is the same in these situations. Namely, the height of the barriers is proportional to the area under the droplet, the height of the columns, their perimeter and their density. Proper understanding of the energy barriers is the key for studying water-repellent properties of biological surfaces and for designing sustainable superhydrophobic surfaces for microdevices, nano and biotechnology, energy and other applications.

References

Barthlott W and Neinhuis C 1997 Purity of the sacred lotus, or escape from contamination in biological surfaces *Planta* **202** 1–8

Bartolo D, Bouamrirene F, Verneuil E, Buguin A, Silberzan P and Moulinet S 2006 Bouncing or sticky droplets: impalement transitions on superhydrophobic micropatterned surfaces *Europhys. Lett.* **74** 299–305

Bergeron V, Bonn D, Martin J Y and Vovelle L 2000 Controlling droplet deposition with polymer additives *Nature* **405** 772–5

Bhushan B, Nosonovsky M and Jung Y C 2007 Towards optimization of patterned superhydrophobic surfaces *J. R. Soc. Interf.* **4** 643–8

Bhushan B, Nosonovsky M and Jung Y C 2008 Lotus effect: roughness-induced superhydrophobic surfaces *Nanotribology and Nanomechanics: an Introduction* 2nd edn, ed B Bhushan (Berlin: Springer)

Blossey R 2003 Self-cleaning surfaces—virtual realities *Nat. Mater.* **2** 301–6

Bormashenko E, Bormashenko Y, Whyman G, Progreb R, Musin A, Jager R and Barkay Z 2008 Contact angle hysteresis on polymer substrates established with various experimental techniques, its interpretation, and quantitative characterization *Langmuir* **24** 4020–5

Fratzl P 2007 Biomimetic materials research: what can we really learn from nature's structural materials? *J. R. Soc. Interface* **4** 637–42

Israelachvili J N 1992 *Intermolecular and Surface Forces* 2nd edn (London: Academic)

Johnson R E and Dettre R H 1964 Contact angle hysteresis *Contact Angle, Wettability, and Adhesion* (*Adv. Chem. Ser.* vol 43) ed F M Fowkes (Washington, DC: American Chemical Society) pp 112–35

Jung Y C and Bhushan B 2008a Wetting behavior during evaporation and condensation of water microdroplets on superhydrophobic patterned surfaces *J. Microsc.* **229** 127–40

Jung Y C and Bhushan B 2008b Dynamic effects of bouncing water droplets on superhydrophobic surfaces *Langmuir* **24** 6262–9

Lafuma A and Quéré D 2003 Superhydrophobic states *Nat. Mater.* **2** 457–60

Li W and Amirfazli A 2006 A thermodynamic approach for determining the contact angle hysteresis for superhydrophobic surfaces *J. Colloid Interface Sci.* **292** 195–201

Marmur A 2006 Underwater superhydrophobicity: theoretical feasibility *Langmuir* **22** 1400–2

Nosonovsky M and Bhushan B 2008a Patterned non-adhesive surfaces: superhydrophobicity and wetting regime transitions *Langmuir* **24** 1525–33

Nosonovsky M and Bhushan B 2008b Biologically-inspired surfaces: broadening the scope of roughness *Adv. Funct. Mater.* **18** 843–55

Nosonovsky M and Bhushan B 2008c Superhydrophobic surfaces for energy conversion and conservation applications *J. Adhes. Sci. Technol.* at press

Nosonovsky M and Bhushan B 2008d *Multiscale Dissipation Mechanisms and Hierarchical Surfaces: Friction, Superhydrophobicity, and Biomimetics* (Heidelberg: Springer)

Quéré D 2005 Non-sticking drops *Rep. Prog. Phys.* **68** 2495–532

Wagner P, Furstner R, Barthlott W and Neinhuis C 2003 Quantitative assessment to the structural basis of water repellency in natural and technical surfaces *J. Exp. Bot.* **54** 1295–303